Translocation of a forced polymer chain through a crowded channel

2014 EPL 106 18003

(http://iopscience.iop.org/0295-5075/106/1/18003)

A Letters Journal Exploring the Frontiers of Physics

April 2014

EPL, **106** (2014) 18003 www.epljournal.org
doi: 10.1209/0295-5075/106/18003

Translocation of a forced polymer chain through a crowded channel

Jiang-Xing Chen[1,2(a)], Jin-Xing Zhu[3], Yu-Qiang Ma[1(b)] and Jian-Shu Cao[2(c)]

[1] *National Laboratory of Solid State Microstructures and Department of Physics, Nanjing University Nanjing 210093, China*
[2] *Department of Chemistry, Massachusetts Institute of Technology - Cambridge, MA 02139, USA*
[3] *Department of Physics, Hangzhou Dianzi University - Hangzhou 310018, China*

received 6 February 2014; accepted in final form 20 March 2014
published online 1 April 2014

PACS 87.15.A- – Theory, modeling, and computer simulation
PACS 87.15.H- – Dynamics of biomolecules
PACS 36.20.-r – Macromolecules and polymer molecules

Abstract – We construct a coarse-grained model in terms of the multiple particles collision (MPC) method to study the translocation dynamics of a linear polymer through a crowded channel full of fixed obstacles. The influences of a crowded environment are focused on. We explore the power-law dependence of the polymer mobility coefficient on its length and on the crowded environment. It is shown that the crowded environment may benefit the length-dependent separation of polymer chains. The exponents characterizing the power-law behavior are discussed to distinguish different dynamical regimes. The properties of the translocating polymer, such as trajectory, moving configuration, and radius of gyration, are investigated. The influences of the radius of obstacles and hydrodynamics interaction on the translocating process are also studied. We believe our studies can shed light on the understanding of complex transport processes in many biological systems.

Introduction. – The translocation of a polymer chain through a constriction is a ubiquitous process in nature, which can be observed in many chemical and biological processes, such as the transport of protein through membrane channels, the motion of DNA and RNA across narrow pores, and the infection of virus into the cell nucleus [1–3]. Also, there are diverse potentially industrial and technical applications like information storage on macromolecules, rapid DNA sequencing, and genomic partitioning techniques [4–7]. Therefore, the physical understanding of the fundamental translocation process is quite important, which has attracted increasing attention in experiments [2,3], simulations [8,9], and theoretical works [10,11].

An external field is widely employed to drive a polymer chain through a channel in which the conformational entropy of the chain is reduced to overcome the resulted entropic barrier and to hasten the translocation [12–14]. Great strides have been made in this field. Kasianowicz *et al.* [3] found that the duration of a driven polymer across a narrow ion channel in a lipid bilayer membrane was proportional to the mean polymer length. Loebl *et al.* [9] reported that the translocation time τ depends on temperature T in a nontrivial relation $\tau \propto T^{1.4}$. Recently, Guo *et al.* [15] simulated the translocation of polymer chains driven through a channel by a solvent flow field in terms of the dissipative particle dynamics approach. They found that τ *vs.* the polymer chain length N satisfies a power law $\tau \propto N^{1.152}$. Using a Monte Carlo simulation, Das *et al.* [16] studied the translocation of polymer chains driven by an electric field and presented a scaling relation $\tau \propto N^{0.674}$. However, the dynamics of polymer translocation through a channel is still quite open.

Intracellular environments are characterized by a high total macromolecular content, known as macromolecular crowding [17,18]. A broad and poorly understood form of dynamics is that of a polymer chain translocating in crowded biological systems. The crowded environment may greatly affect the translocation dynamics. For example, the matrix of obstacles may control the properties of a polymer chain including diffusion [19,20], configuration [21,22], and relaxation [23,24] as the occupied volume fraction of obstacles is varied. On the other hand,

(a) E-mail: jxchen@hdu.edu.cn
(b) E-mail: myqiang@nju.edu.cn
(c) E-mail: jianshu@mit.edu

most studies arise from a particular application in separation mechanisms designed to characterize polymers by molecular weight, charge, or radius of gyration according to their transport properties in the matrix of obstacles, packed column, and other tortuous media [25–27]. The most well-developed method is DNA gel electrophoresis separation where three regimes, *i.e.* Ogston, reptation, and entropic-trapping (ET), were displayed based on the size dependence between the polymers and the mean gel pore [25]. Driving DNA using an electric field through postarrays is another well-known micro-fluidic method for separating long DNA by size [28]. The hooking of DNA on arrays and subsequent length-dependent unhooking underpins the separation mechanism.

When a polymer chain is driven through a crowded channel, the dynamics of translocation may be more complex since the motion of a polymer is both constricted by the channel and the crowded environment. The nature of the forced movement of a polymer chain in a random crowded channel is still far from being well understood. In this paper, we construct a channel model crowded with spherical objects. A linear polymer chain is forced by an external electric field to translocate the crowded channel. The properties of translocation are studied in terms of a mesoscopic description with explicit solvent molecules.

Mesoscopic model. –

Polymer chain model. A standard bead-spring model of a linear polymer chain with N_b beads is utilized in our simulation. The interactions among the polymer beads consist of a bead-spring potential between neighboring beads as well as bead-bead interactions among all beads. The non-Hookian bead-spring potential is given by finite extensible nonlinear elastic (FENE) interactions,

$$V_{FENE}(r) = -\frac{k}{2} r_0^2 \ln\left[1 - \left(\frac{r}{r_0}\right)^2\right], \quad r < r_0, \qquad (1)$$

where $k = 30\epsilon/\sigma_b$, ϵ is an energy parameter, σ_b is the bead diameter, $r = |\mathbf{r}_i - \mathbf{r}_j|$ is the distance between neighboring beads, and $r_0 = 1.5\sigma_b$ is its maximum value.

The repulsive Lennard-Jones (LJ) potential among all beads is used to consider exclusive volume,

$$V_{LJ}(r) = 4\epsilon\left[\left(\frac{\sigma_b}{r}\right)^{12} - \left(\frac{\sigma_b}{r}\right)^{6} + \frac{1}{4}\right], \quad r < r_c, \qquad (2)$$

and zero otherwise. Here $r_c = 2^{1/6}\sigma_b$ is a cut-off distance.

Obstacles and solvent molecules model. The environment of crowding agents is formed by N_o stationary spherical objects with radius R_o (see fig. 1). Crowding effects are studied by changing the volume fraction ($\phi = 4\pi N_o R_o^3/3V$) and radius of the obstacles.

To properly account for solvation and collective hydrodynamic effects, we make use of a mesoscopic multiparticle collision (MPC) description of the solvent dynamics [29,30]. In MPC dynamics, N_s point solvent

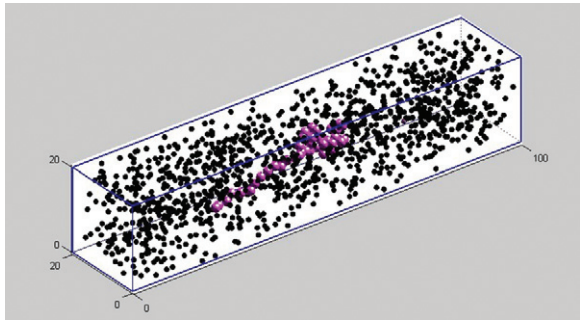

Fig. 1: (Color online) Instantaneous configuration of the simulation model. The black spheres denote the randomly distributed stationary obstacles. The red spheres show the translating polymer chain. Solvent molecules are not shown here.

particles with velocity $\mathbf{v}_i(t)$, representing coarse-grained real molecules, free stream and undergo effective collisions at discrete time intervals t_{MPC}, accounting for the effects of many real collisions during this time interval. The system is partitioned into many cubic cells (with length $a_0 = 1$) given labels ν and at each time t_{MPC} rotation operator $\hat{\omega}_\nu(\theta)$, chosen at random from a set of rotation operators, are assigned to each cell. The collision rule is applied to calculate the postcollision velocities of the particles,

$$\mathbf{v}_i(t + t_{MPC}) = \mathbf{V}_\nu + \hat{\omega}_\nu(\theta)(\mathbf{v}_i(t) - \mathbf{V}_\nu), \qquad (3)$$

where $\mathbf{V}_\nu$ is the center-of-mass velocity of the cell ν. MPC dynamics conserves mass, momentum and energy as well as phase-space volumes. Because the dynamics preserves the basic conservation laws, hydrodynamic interactions are properly accounted for and no additional assumptions about friction coefficients or random forces need to be made. The transport properties of the solvent undergoing MPC dynamics can be computed analytically [29–31]. The interactions between solvent-bead, bead-obstacle, and solvent-obstacle are all through repulsive LJ potentials.

Simulation method and details. A channel of volume $V = L_x \times L_y \times L_z$ ($L_y = L_z = 20$ and $L_x = 100$, see fig. 1) is simulated. An external electric field $\mathbf{E}$ is applied in the x-direction in which a periodic boundary condition is used. In the y and z directions, the bounce-back rule is used to realize a no-slip boundary condition. The obstacles and solvent molecules are placed in the channel with randomly chosen positions, avoiding overlapping configurations. A polymer chain is randomly placed in another channel with the same size but without obstacles. After long time evolution, it was forced by a weak electric field to the crowded channel slowly. We start the time when the center of mass $\mathbf{r}_{cm}$ enters into the $x = 0$ of the crowded channel and record the translocation time at τ when $\mathbf{r}_{cm}$ reaches the point $x = L_x$. The initial velocities of all mobile molecules were chosen from a Maxwell-Boltzmann distribution characterized by the system temperature T.

Once ϕ is fixed, the number of obstacles and solvents can be computed by the relations $N_o = 3V\phi/(4\pi R_o^3)$ and

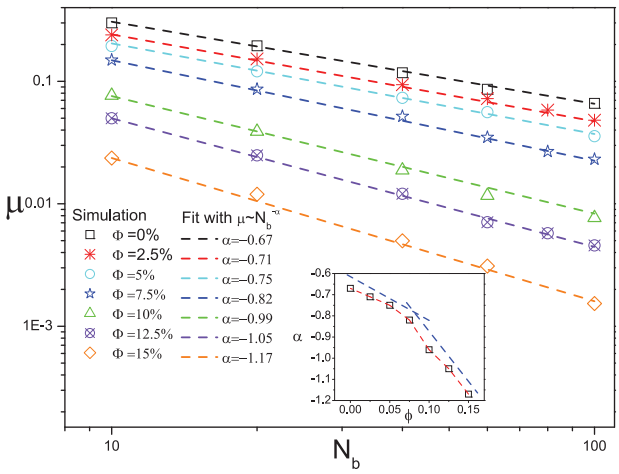

Fig. 2: (Color online) The dependence of the mobility coefficient (μ) of a polymer chain on its length (N_b) and volume fraction of obstacles (ϕ). The dots from the simulation are fitted by dashed lines with a power law $\mu \sim N_b^{\alpha}$. The inset shows the relation between the exponent α and ϕ. Two dashed lines are displayed to guide the different slopes. The data is an average of 40 realizations.

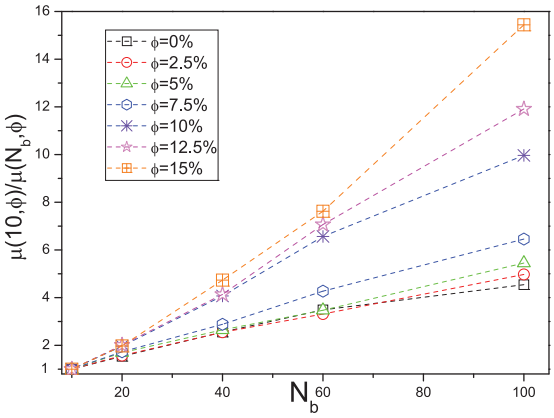

Fig. 3: (Color online) The ratio of the mobility coefficient $\frac{\mu(10,\phi)}{\mu(N_b,\phi)}$. $\mu(N_b,\phi)$ is a function of the polymer length N and of the obstacle volume fraction ϕ.

$N_s = n_s V(1-\phi)$ where $n_s = 8$ is fixed, respectively. The length of the polymer chain varies: $N_b = 10, 20, 40, 60$, and 100. The mass of a bead obeys the relation $m_b = n_s \pi \sigma_b^3/6$ according to its volume to ensure that the polymer is approximately neutrally buoyant.

The full dynamics of the system is then carried out using the hybrid MD-MPC dynamics. The MD time step t_{MD} used to integrate Newtons equations of motion with the velocity Verlet algorithm is $t_{MD} = 0.01$. Multiparticle collisions with rotations angle $\theta = \pi/2$ are carried out every 100 MD steps so that $t_{MPC} = 1.0$. Random shifts of the grid defining the collision cells are also applied, so that Galilean invariance is ensured.

All quantities are reported in dimensionless units based on energy ϵ, solvent mass m_s, and cell length a_0 parameters: $r/a_0 \to r$, $t(\epsilon/m/a_0^2)^{1/2} \to t$, and $k_B T/\epsilon \to T$. Simulation parameters are: $m_s = 1.0$, $\sigma_b = 1.0$, $T = 1/3$, and $R_0 = 0.5$.

Results and discussions. – In fig. 2, we present the dependence of the mobility coefficient μ on the length of the polymer chain N_b under different obstacle volume fraction ϕ. The data μ is obtained from the relation $\mu = L_x/E\tau$. It is obvious that the increases of ϕ and N_b both decrease the value of $\mu(N_b,\phi)$. A main result is that the power-law behavior $\mu \sim N_b^{\alpha}$ is obtained at any ϕ. At $\phi = 0$, we find that the exponent is $\alpha = -0.67$ which is close to the value $\alpha = -0.674$ reported by Das *et al.* in a recent study simulating a polymer chain through a narrow channel. When the channel becomes crowded (the value of ϕ is increased), the exponents are decreased from $\alpha > -1.0$ to $\alpha < -1.0$ (see the case $\alpha = -1.17$ at $\phi = 0.15$). The α-ϕ dependence is plotted in the inset of fig. 2 in which it is shown that the values of α decrease faster when ϕ is bigger.

At each ϕ, we select the mobility of short polymer chain with 10 beads, *i.e.* $\mu(10,\phi)$ as a standard of reference. We compare the $\mu(N_b,\phi)$ at different N_b in fig. 3 when the degree of crowding is changed. With the increasing of polymer length, the ratios $\frac{\mu(10,\phi)}{\mu(N_b,\phi)}$ are increased (see fig. 3). That means the polymers can be separated depending on their lengthes. However, the ratio is small for small ϕ, which makes the separation difficult. For example, the values of $\frac{\mu(10,0)}{\mu(N_b,0)}$ vary only from 1.0 to 4.4 when N_b is increased from 10 to 100 (see the corresponding value $\frac{\mu(10,0)}{\mu(100,0)} = 4.4$). Similar examples with $\alpha > -1.0$ ($\phi = 0.025, 0.05$, and 0.075) are also illustrated in fig. 3. When $\alpha < -1.0$, the values $\frac{\mu(10,\phi)}{\mu(N_b,\phi)}$ are greatly increased with N_b. For example, the value of $\frac{\mu(10,0.15)}{\mu(100,0.15)}$ is about 15.5. That means the crowded environment will highly increase the efficiency of separation. We attribute the mechanism why the crowded environment can benefit separating a polymer to the different translocation dynamics regimes resulted from the increase of ϕ.

Depending on the value of α, we roughly divide three dynamical regimes that characterize the translocation of a polymer chain in a crowded channel. When the exponent $\alpha > -1.0$, the volume fraction is small, *e.g.* $\phi = 0.05$, the moving polymer chain is confined in the environment formed by the channel and sparse obstacles. The polymer enters into voids of typical size comparable to or larger than their size. In transition between these voids the chains have to overcome entropic barriers which are set up due to reduction of their possible configurations [32]. It is an entropy-confined regime, since the entropy configuration dominates the dynamical behavior. The simulation result in fig. 4(a) shows that the size of the moving chain indicated by the averaged mean square radius of gyration $\langle R_g \rangle$ is a nonmonotonic function of the obstacle volume fraction ϕ. When ϕ is increased not too much, *e.g.* from 0 to 0.025, the chain size $\langle R_g \rangle$ decreases slightly. Since the chain confined by the channel is sill coiled so far, this effect results from the compression of the increased

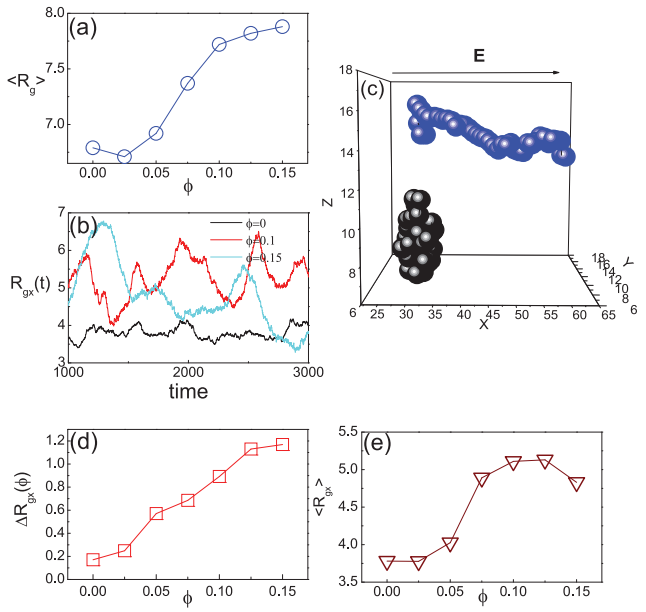

Fig. 4: (Color online) (a) Averaged mean square radius of gyration $\langle R_g \rangle = \frac{1}{N}\sum_{n=1}^{N} R_g(nt_{MD})$ as a function of ϕ. Here, $R_g(nt_{MD})$ is the mean square radius of gyration defined by $R_g(t) = \frac{1}{N_b}\sum_{i=1}^{N_b}(\mathbf{r}_i(t) - \mathbf{r}_{cm}(t))^2$ at the time $t = nt_{MD}$ and $N = \tau/t_{MD}$. (b) Evolutions of $R_{gx}(t)$ in the x-direction with $\phi = 0$, 0.1 and 0.5 are shown, respectively. (c) Plotted instantaneous moving configurations with $\phi = 0.15$ at different times. (d) Standard deviation $\Delta R_{gx}(\phi) = \frac{1}{N}\sqrt{\sum_{n=1}^{N}(R_{gx}(t) - \langle R_{gx}\rangle)^2}$. (e) Averaged mean square radius of gyration in the x-direction $\langle R_{gx}\rangle = \frac{1}{N}\sum_{n=1}^{N} R_{gx}(nt_{MD})$ as a function of ϕ. The data is an average of 40 realizations. Other parameters: $N_b = 40$ and $E = 0.25$.

obstacles surrounding around the moving polymer. The external electric field facilitates this effect to force the polymer into voids among the obstacles to compress it. This phenomenon was also observed in pervious studies simulating the diffusion of a polymer in porous materials by MD simulations [33] and MC simulations [32]. In this dynamical regime, the beads in the polymer chain move collectively as a whole. The chain does not stretch in the x-direction so much, which has been shown in fig. 4(b) where the values of $R_{gx}(t)$ are small. The collective motion is also confirmed by the small standard deviation of $\Delta R_{gx}(\phi)$ in fig. 4(d). The trajectories of the center of mass with different ϕ are plotted in fig. 5. In this regime (see the cases with $\phi = 0$ or $\phi = 0.05$), the polymer can diffuse in the direction perpendicular to the external field with consequent fluctuation shown by Y_{cm}.

In the vicinity of $\alpha = -1.0$ ($\mu \sim N_b^{-1}$), the voids among obstacles are small (ϕ is now increased) so that they are difficult to accommodate the coiled polymer chain. Both topological hindrances and entropic effects play important roles. Consequently, the beads of polymer snakes through those small voids, which elongate the polymer chain in the x-direction. This behavior is similar to the reptation regime observed in the gel electrophoresis [25]. From

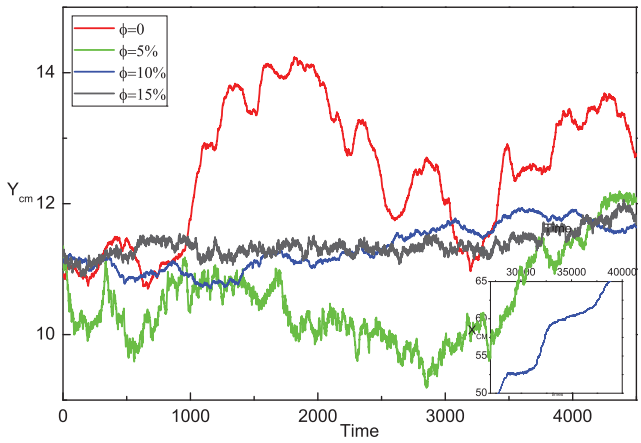

Fig. 5: (Color online) (a) The evolution of the trajectories of the center of mass in the y-direction $Y_{cm}(t)$ with different $\phi = 0$, 0.05, 0.1, and 0.15 for $N_b = 40$ and $E = 0.25$. The inset is the evolution of the center of mass in the x-direction $x_{cm}(t)$ with $\phi = 0.15$. The data are an average of 40 realizations.

fig. 4(a) and (e), one can find that $\langle R_g \rangle$ and $\langle R_{gx} \rangle$ both increase fast with ϕ. The values of $R_{gx}(t)$ show obvious fluctuation (see the example of $\phi = 0.1$ in fig. 4(b)). In fig. 4(d), the dependence of the standard deviation $\Delta R_{gx}(\phi)$ on ϕ is monotonic. And, the $Y_{cm}(t)$ is severely restricted by the increased obstacles (see the example with $\phi = 0.1$ in fig. 5).

When ϕ is increased further so that α is smaller than -1.0, the channel becomes more and more crowded. Accordingly, Y_{cm} in fig. 5 shows that the trajectory of the center of mass looks like a one-dimensional motion. In some places, the voids among the obstacles are so small that a part of moving beads are difficult to pass through those regions. Then, the polymer is blocked, which will result in a contracted configuration. Gradually, the beads adjust themselves under the forcing of the external electric field until they find voids to stretch into with a stretched configuration. An example is shown in fig. 4(c) where an instantaneous contracted and a stretched configuration are presented from the simulation. Accompanying with the contract-stretch process, $R_{gx}(t)$ shows a large fluctuation (see the case $\phi = 0.15$ in fig. 4(b)). One can see that $R_{gx}(t)$ at $\phi = 0.15$ is even smaller than in the case with $\phi = 0$ at $t = 2850$. Consequently, a knee point in the $\langle R_{gx}\rangle$-ϕ curve occurs, which can be seen from fig. 4(e).

Thus, the third regime with $\alpha < -1.0$ is a worm-like regime. In the reptation regime, once a bead finds a void bigger than itself, it will enter into the void. Thus, the motion of the beads looks individual, which may be indicated by the continuous velocity. However in the worm-like regime, the small voids block the polymer chain with contracted configurations for a long time until the chain finds ways to collectively pass through with a stretched configuration. Accordingly, obvious steps are observed in the velocity curve (see the inset of fig. 5).

Therefore, the division of dynamical regimes based on α reflects the degree of crowding and structure of the

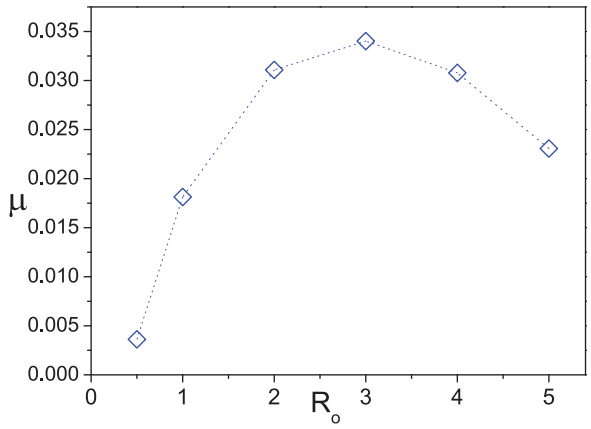

Fig. 6: (Color online) The dependence of the mobility coefficient μ on the radius of obstacles in a given crowded channel $\phi = 0.15$. The strength of the electric field is $E = 1.25$ and the length of the chain is $N_b = 60$.

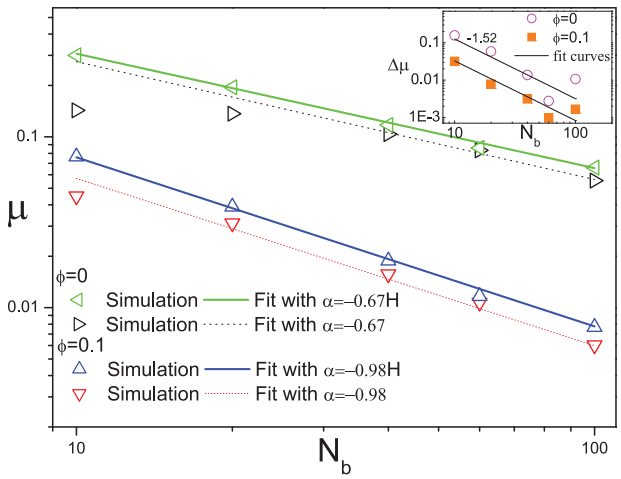

Fig. 7: (Color online) Comparison of the polymer mobility μ with and without HI under different ϕ ($\phi = 0$ and $\phi = 0.1$) and N. The triangles are plotted from the simulation while the lines are the corresponding fit curves. Inset: the corresponding difference of mobility ($\Delta\mu$) with and without HI.

obstacle array as ϕ is increased, and the interaction between polymers with different length and voids with different sizes. Strictly speaking, the division is tentative and rough. However, at least, the simulation contributes to understand the translocation dynamics of a polymer chain in a crowded channel, since it catches their characteristics and distinguishes them upon increasing crowding environment.

Based on the discussion about the dynamical regimes, the mechanism which underpins the length-dependent separation is illustrated. The effects of a crowded environment on a longer polymer are more pronounced. For a short chain, it is not difficult to find voids among obstacles to pass through when ϕ is increased. However, for a long chain, it undergoes the three dynamics regimes mentioned above. Thus, when ϕ is increased, the degree of the decreased mobility coefficient is more obvious as the length of the polymer is increased.

The mobility coefficient μ also depends on the radius of the obstacles R_o when the volume fraction ϕ is fixed (see fig. 6). Both ϕ and R_o control the sizes of the voids in the random array of obstacles. As R_o increases for fixed ϕ, the number of obstacles is decreased. Accordingly, the characteristic void size increases, that will release the polymer chain from a snake-like chain to a coiled configuration. Accordingly, the value of μ increases with R_o. Since a coiled polymer may roll off on an big obstacle [34], the slope of the μ-R_o curve becomes small as R_o is increased and it ultimately reaches a peak value in a certain R_o. Then, μ decreases, which results from two reasons. One is that the polymer may hook on large obstacles near the wall of the channel. Another is that large obstacles may block the channel.

Then, we study the influence of the hydrodynamic interaction (HI) effect in polymer translocation. In our hybrid MD-MPC simulation, the polymer exchanges momentum with the solvent by explicit bead-solvent interactions. These bead-solvent interactions capture some features of the solvent structure in the vicinity of the polymer chain. For example, flow vortexes may be formed behind the moving polymer beads, which leads to long-range HI between beads with consequent increase of their mobilities. If HI are suppressed, each polymer bead acts as an independent source of friction; consequently, the frictional force on the polymer is much larger when hydrodynamic effects are neglected. HI may be eliminated in the simulations by replacing the MPC dynamics by random sampling of the postcollision velocities from a Boltzmann distribution. This random sampling destroys local momentum conservation and velocity correlations in the solvent which are responsible for HI.

We compare the mobility of the polymer with and without HI under different ϕ and N_b in fig. 7. It is confirmed by simulation that HI leads to bigger μ, which indicates that the polymer passes through the channel faster. Another phenomenon is that the difference of μ induced by HI is obvious when N_b is small, *e.g.* $N_b = 10$, 20. The $\Delta\mu$-N_b curve in the inset shows that $\Delta\mu$ decreases when N_b is increased. That means HI effects are obvious on short polymers and become weaker on longer polymers. ϕ also plays a role. Given a fixed length of the polymer, *e.g.* $N_b = 20$ in the inset, the value of $\Delta\mu$ under $\phi = 0.1$ is much smaller than that under $\phi = 0$. This illustrates that HI are expected to be screened by the presence of obstacles. For $\phi = 0.1$ and $N_b = 100$, the difference $\Delta\mu$ can almost be neglected. It seems that another power law $\Delta\mu \sim N_b^{-1.52}$ with exponent independent of ϕ can be obtained (see the fit curves in the inset). Within the regime where HI are screened when N_b is bigger enough, the power law $\mu \sim N_b^{\alpha}$ is obtained again (see the dotted lines in fig. 7), although there are big deviations when N_b is small. One can find that the consistence of the power law is better when ϕ is bigger in fig. 7. The exponent α under a given ϕ is the

same with and without HI ($\alpha = -0.67$ with $\phi = 0$ and $\alpha = -0.98$ with $\phi = 0.1$), showing that it also does not depend on the HI.

It is known that structural elements in the cell environment form a quite crowded network which may be considered stationary on the time scales of interest [17,18]. The study of polymers in such fixed disordered obstacles is a fundamental problem in its own right [21–24]. If the obstacles are mobile, the confinement from the surrounding background will not be so strong as that in this simulation. The polymer chain may push and drag obstacles when it moves. The motion of the driven polymer may also induce strong HI among obstacles. Apparently, the moving configuration will be quite different. Consequently, the properties of translocation, *e.g.* scaling behavior, may be changed and different from those in this simulation.

Conclusion. – In conclusion, we construt a mesoscopic model to study the translocating dynamics of a driven polymer chain through a crowded channel. The dependence of the mobility μ on the polymer length N_b and on the obstacle volume fraction ϕ is simulated. A power law μ-N_b^{α} is presented. We find that the crowded channel can greatly increase the efficiency of separating the polymer chain depending on length. In terms of the exponent α, three tentative dynamical regimes, entropy-confined, reptation, and worm-like, are divided to characterize the translocating behavior when ϕ is increased. The mechanism of separation is discussed based on the dynamical regimes. When the radius of obstacles is increased for a fixed ϕ, the mobility μ increased firstly and then decreased. Compared with the condition without HI, the HI effects will increase the mobility. The difference of mobility $\Delta\mu$ is big if the chain is short while it is small with a long chain. The matrix of obstacles screens the HI, which make $\Delta\mu$ decrease with big ϕ. A power law $\Delta\mu \sim N_b^{-1.52}$ is presented. We believe our results will shed light on the understanding of translocation dynamics in this field.

* * *

This work was supported by the National Natural Science Foundation of China (Nos. 91027040, 10974080), National Basic Research Program of China (No. 2012CB821500), the Natural Science Foundation of Zhejiang Province (No. LY13A040007), and China Postdoctoral Science Foundation (No. 2013M541634).

REFERENCES

[1] Alberts B., Johnson A., Lewis J., Raff M., Roberts K. and Walter P., *Molecular Biology of the Cell*, 4th edition (Garland Science, New York) 2002.
[2] Meller A., Nivon L. and Branton D., *Phys. Rev. Lett.*, **86** (2001) 3435.
[3] Kasianowicz J. J., Brandin E., Branton D. and Deamer D. W., *Proc. Natl. Acad. Sci. U.S.A.*, **93** (1996) 13770.
[4] Bayley H. and Cremer P. S., *Nature (London)*, **413** (2001) 226.
[5] Li J. L., Gershow M., Stein D., Brandin E. and Golovschenko J. A., *Nat. Mater.*, **2** (2003) 611.
[6] Douville N., Huh D. and Takayama S., *Anal. Bioanal. Chem.*, **391** (2008) 2395.
[7] Reisnera W., Larsenb N. B., Silahtaroglud A., Kristensenb A., Tommerupd N., Tegenfeldtc J. O. and Flyvbjergb H., *Proc. Natl. Acad. Sci. U.S.A.*, **107** (2007) 13294.
[8] Muthukumar M. and Kong C. Y., *Proc. Natl. Acad. Sci. U.S.A.*, **103** (2005) 5273.
[9] Loebl H. C., Randel R., Goodwin S. P. and Matthai C. C., *Phys. Rev. E*, **67** (2003) 041913.
[10] Matysiak S., Montesi A., Pasquali M., Kolomeisky A. B. and Clementi C., *Phys. Rev. Lett.*, **96** (2006) 118103.
[11] Muthukumar M., *Electrophoresis*, **23** (2003) 1417.
[12] Luo K., Ala-Nissila T., Ying S. C. and Metzler R., *EPL*, **88** (2009) 68006.
[13] Reccius C. H., Stavis S. M., Mannion J. T., Walker L. P. and Craighead H. G., *Biophys. J.*, **95** (2008) 273.
[14] Storm A. J., Storm C., Chen J. H., Zandbergen H., Joanny J. F. and Dekker C., *Nano Lett.*, **5** (2005) 1193.
[15] Guo J. Y., Li X. J., Liu Y. and Liang H. J., *J. Chem. Phys.*, **134** (2011) 134906.
[16] Das A. K. and Hong P. D., *Polymer*, **51** (2010) 2244.
[17] Fulton A. B., *Cell*, **30** (1982) 345.
[18] Record T. M. jr., Courtenay E. S., Caley S. and Guttman H. J., *Trends Biochem. Sci.*, **23** (1998) 190.
[19] Echeverria C. and kapral R., *Phys. Chem. Chem. Phys.*, **14** (2012) 6755.
[20] Verkman A. S., *Trends Biochem. Sci.*, **27** (2002) 27.
[21] Chang R. and Yethiraj A., *J. Chem. Phys.*, **126** (2007) 174906.
[22] Sung B. J., Chang R. and Yethiraj A., *J. Chem. Phys.*, **130** (2009) 124908.
[23] Chang R. and Yethiraj A., *Phys. Rev. Lett.*, **96** (2006) 107802.
[24] Chern S. and Coalson R. D., *J. Chem. Phys.*, **111** (1999) 1778.
[25] Rousseau J., Drouin G. and Slater W., *Phys. Rev. Lett.*, **79** (1997) 1945.
[26] Volkmuth W. D. and Austin R. H., *Nature*, **358** (1992) 600.
[27] Reichhardt C. J. Olson and Reichhardt C., *Phys. Rev. E*, **74** (2006) 051908.
[28] Doyle P. S., Bibette J., Bancaud A. and Viovy J. L., *Science*, **295** (2002) 2237.
[29] Kapral R., *Adv. Chem. Phys.*, **140** (2008) 89.
[30] Gompper G., Ihle T., Kroll D. M. and Winkler R. G., *Adv. Polym. Sci.*, **221** (2009) 1.
[31] Ihle T. and Kroll D., *Phys. Rev. E*, **67** (2003) 066706; Ihle T., Tuzel E. and Kroll D., *Phys. Rev. E*, **72** (2005) 046707.
[32] Yamakov V. and Milchev A., *Phys. Rev. E*, **55** (1997) 1704.
[33] Chang R. and Yethiraj A., *J. Chem. Phys.*, **126** (2007) 174906.
[34] Saville P. M. and Sevick E. M., *Macromolecules*, **32** (1999) 892.